Inorganic Chemistry

Article

pubs.acs.org/IC

# Probing the Influence of Phosphonate Bonding Modes to Uranium(VI) on Structural Topology and Stability: A Complementary Experimental and Computational Investigation

Tao Zheng,[†,‡,Δ] Qun-Yan Wu,[§,Δ] Yang Gao,[†,‡] Daxiang Gui,[†,‡] Shiwen Qiu,[†,‡] Lanhua Chen,[†,‡] Daopeng Sheng,[†,‡] Juan Diwu,*[,†,‡] Wei-Qun Shi,*[,§] Zhifang Chai,[†,‡] Thomas E. Albrecht-Schmitt,[∥] and Shuao Wang*[,†,‡]

[†]School for Radiological and Interdisciplinary Sciences (RAD-X) and [‡]Collaborative Innovation Center of Radiation Medicine of Jiangsu Higher Education Institutions, Soochow University, Suzhou, Jiangsu 215123, China

[§]Key Laboratory of Nuclear Radiation and Nuclear Energy Technology and Key Laboratory For Biomedical Effects of Nanomaterials and Nanosafety, Institute of High Energy Physics, Chinese Academy of Sciences, Beijing 100049, China

[∥]Department of Chemistry and Biochemistry, Florida State University, 95 Chieftain Way, Tallahassee, Florida 32306, United States

Supporting Information

**ABSTRACT:** Systematic control of the reactions between U(VI) and 1,4-phenylenebis(methylene))bis(phosphonic acid) (**pmbH$_4$**) allows for alterations in the bonding between these constituents and affords three uranyl phosphonate compounds with chiral one-dimensional (1D), two-dimensional (2D), and three-dimensional (3D) structures, namely, [TPA][$UO_2$(pmbH$_3$)(pmbH$_2$)$H_2O$]·2$H_2O$ (**1**), [$NH_4$]$_2$[$UO_2$(pmb)] (**2**), $UO_2$(pmbH$_2$) (**3**), and the first uranyl mixed phosphite/phosphonate compound [TMA]$_2$[($UO_2$)$_2$(pmb)($HPO_3$)] (**4**) (TPA = $NPr_4^+$, TMA = $NMe_4^+$). These compounds crystallize in the space groups $P2_12_12_1$, $P\bar{1}$, $P2_1/c$, and *Cmcm*, respectively. Further investigation of the local uranyl coordination environment reveals that in **1** only oxygen atoms from P═O moieties ligate the uranium centers; whereas in **2** only P−O$^-$ oxygen atoms are involved in bonding and yield a layered topology. Compound **3** differs sharply from the first two in that conjugated P═O and P−O$^-$ oxygen atoms chelate the uranium centers resulting in a 3D framework. In compound **4**, a phosphonate group bridges three uranyl centers further coordinated with a phosphite ligand $HPO_3^{2-}$, which is a product of pmbH$_4$ decomposing, forming a 2D layered structure. Compounds **3** and **4** also contain a different coordination environment for U(VI) than that found in **1** or **2**. In this case, tetragonal bipyramidal $UO_6$ units occur instead of the far more common $UO_7$ pentagonal bipyramids found in **1** and **2**. Interestingly, **1** converts to **3** at elevated reaction temperatures, indicating that the formation of **1** is likely under kinetic control. This is supported by thermal analysis, which reveals that **3** has higher thermal stability than **1** or **2**. UV−vis−near-IR absorption and fluorescence spectroscopy show that the absorption and photoluminescence intensity increases from **1** to **4**. Density functional theory electronic structure calculations provide insight into the nature of the interactions between U(VI) and the phosphonate ligands.

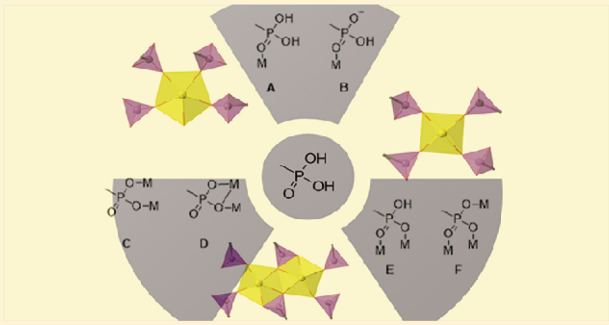


## INTRODUCTION

The interaction of oxo donor atoms from phosphorus oxoanions with uranium and other f-elements is a key component of environmental transport,[1] mineralogy,[2] the nuclear fuel cycle,[3] materials development,[4] and coordination chemistry.[5] Biphasic extractants such as tributyl phosphate (TBP)[3b,6] and octyl(phenyl)-*N*,*N*-diisobutylcarbomoylmethylphosphine oxide (CMPO),[3f,7] which contain P═O functional groups, play crucial roles in the recycling of used nuclear fuel. However, the nature of bonding between these ligands and f-elements is still in need of further development owing in part to the real complexities of an ostensibly simple system.[3] In the PUREX and related processes the P═O moiety is used to coordinate U(VI) and Pu(IV); the persistence of this interaction at low pH is among the most important aspects of this chemistry.[8] Further investigation of related phosphonates eventually led to the development of diphosphonates, most notably methylenediphosphonic acid, tethered to polymer backbones, that is, Diphonix resins. These resins are used to strip low levels of actinide ions from effluents from nuclear facilities; such processing is often referred to as polishing.[9] However, the differences between the TBP and CMPO-type phosphorus-oxo functionality with that of phosphonic acids has

**Received:** January 7, 2015
**Published:** March 27, 2015





DOI: 10.1021/acs.inorgchem.5b00024
*Inorg. Chem.* 2015, 54, 3864−3874

led to some debate over the nature of coordination of the diphosphonates group in Diphonix resins to actinide ions because this unit could utilize P−O$^-$ moieties instead of P═O groups as shown in Scheme 1.

**Scheme 1. Possible Bonding Modes of the Diphosphonic Acids to Actinide Ions**

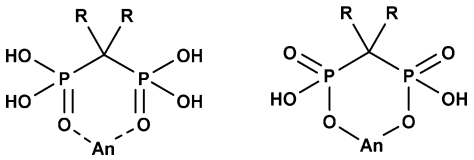


Uranium normally competes with protons to bond with either P−O$^-$ or P═O oxygen atoms within phosphonate groups. Owing to the negative charge on the P−O$^-$ group, its coordinating ability to cationic metal ions originates primarily from electrostatic forces, whereas the neutral P═O group possesses lone pairs of electrons that can be donated into empty valence orbitals of U(VI). Therefore, pH affects the coordination ability of P−OH to a much greater extent than that of P═O. It is important to understand the coordinating competition between P═O and P−O$^-$ groups toward actinides under specific conditions to better design and develop nuclear separation and remediation strategies. One way to do this is by carefully examining the bonding modes within actinide phosphonate materials that contain both P═O and P−O$^-$ groups.

Numerous actinide phosphonate compounds have been prepared and characterized over the past several decades. The majority of these contain U(VI), but Th(IV) and transuranium examples are becoming better represented.[5,10] Actinides in the VI oxidation state are normal found within linear dioxo actinyl units where additional donor atoms are forced to bond in the equatorial plane perpendicular to the actinyl unit, typically resulting in layered structures.[11] One-dimensional (1D) and three-dimensional (3D) topologies that contain actinyl cations are less common. Notably, only two diphosphonate ligands have been demonstrated thus far to be able to form topologies of all possible dimensionalities: (1-hydroxyethane-1,1-diyl)bis(phosphonic acid) (**iopH$_4$**)[12] and 1,4-phenylenebis(phosphonic acid) (**1,4-bdpH$_4$**).[4e,13] 1D chain and nanotube structures were found in (Hbpi)[$(UO_2)(H_2O)$(iopH)]·$H_2O$,[12a] (teah)[$(UO_2)$(4-bdp$H_{2.5}$)$_2$($H_2O$)],[13a] and $Cs_{3.62}H_{0.38}$[$(UO_2)_4$(4-bdp$H_2$)$_3$(4-bdp)$F_2$],[4e] with the last showing a unique nanotubular structure. The corresponding two-dimensional (2D) and 3D topologies were obtained as the phosphonate groups bridged between adjacent layers. The dimensionality of the structure can strongly affect the environmental stability of U(VI) compounds.[14] However, these and other studies have not revealed the role that P−O−U and P═O−U bonding modes plays in these materials. Controlling both the overall topology and the specific coordination features within actinide phosphonates may allow for increasing their stability in waste form and other applications such as proton-conductivity.[15]

Herein, we report on the synthesis, structures, spectroscopy, and quantum mechanical calculations of three uranyl phosphonates with 1D, 2D, and 3D structures, namely, [TPA][$UO_2$(pmbH$_3$)(pmbH$_2$)$H_2O$]·$2H_2O$ (**1**), [$NH_4$]$_2$[$UO_2$(pmb)] (**2**), $UO_2$(pmbH$_2$) (**3**), and the first uranyl mixed phosphite/phosphonate compound [TMA]$_2$[$(UO_2)_2$(pmb)($HPO_3$)] (**4**) (TPA = $NPr_4^+$; TMA = $NMe_4^+$; pmb = 1,4-phenylenebis(methylene)bis(phosphonate).

## EXPERIMENTAL SECTION

***Caution!*** *While all uranium compounds used in these studies contained depleted uranium, standard precautions were performed for handling radioactive materials, and all studies were conducted in a laboratory dedicated to studies on actinide elements.*

**Materials and Methods.** (1,4-phenylenebis(methylene))bis(phosphonic acid) (pmbH$_4$) was synthesized following the procedure reported in the literature.[16] α,α′-Dibromo-*p*-xylene (97%), triethylphosphite, concentrated HCl, $UO_2(NO_3)_2$·$6H_2O$, urea, tetrapropylammonium hydroxide (40% in water), and HF (40%) were used as received. The room-temperature infrared spectra were collected on a Thermo Nicolet 6700 instrument.

**Synthesis.** Compound **1**: A mixture of $UO_2(NO_3)_2$·$6H_2O$ (0.1 mmol, 0.0502 g), **pmbH$_4$** (0.2 mmol, 0.0532 g), tetrapropylammonium hydroxide (0.1 mmol, 0.100 mL), $H_2O$ (2 mL), and two drops of HF (40%) was placed in a 15 mL Teflon-lined stainless steel vessel and heated to 120 °C in 2 h and then cooled to 25 °C in 72 h. The pH before and after heating is in the range of 2.40−2.42 and 2.28−2.55, respectively. Yellow block crystals were collected as a single phase. Yield: 80% (based on uranium). IR (KBr, cm$^{-1}$): 3531−3221(b, m), 2989(m), 2948(m), 2920(m), 2888(m), 2366(b, m), 1683(m), 1643(m), 1514(s), 1488(s), 1408(m), 1254(m), 1201(m), 1152(s), 1124(s), 1084(w), 1065(w), 1021(w), 970(m), 958(m), 920(vs), 845(m), 835(w), 813(w), 796(m), 757(m), 718(w), 689(w), 643(w), 610(m), 564(m), 540(w), 505(m), 450(m). For compound **2**, tetrapropylammonium hydroxide (0.1 mmol, 0.100 mL) was replaced with urea (1.6 mmol, 0.0977 g), and then the mixture was placed in a 15 mL Teflon-lined stainless steel vessel and heated to 200 °C in 2 h, kept there for 72 h, and then cooled to 25 °C at a rate of 5 °C/h. The pH before and after heating is in the range of 2.15−2.18 and 9.35−9.40, respectively. Yellow crystals were collected as a single phase. Yield: 82% (based on uranium). IR (KBr, cm$^{-1}$): 3295(m), 3146−2779(b, s), 1667(m), 1512(m), 1492(m) 1437(s), 1420(s), 1406(s), 1296(w), 1250(m), 1243(m), 1198 (m), 1120(s), 1095(s), 1063(s), 991(s), 947(s), 899(s), 855(s), 827(w), 819(w), 805(m), 737(w), 726(w), 525(s), 565(s), 543(m), 496(m). Compound **3** was obtained by the same procedure as compound **2**, without urea. The pH before and after heating is in the range of 1.76−1.78 and 1.65−1.78, respectively. Yellow rhombic crystals were collected as a single phase. Yield: 69% (based on uranium). IR (KBr, cm$^{-1}$): 3168(b, s), 2922(w), 2173(b, w), 1514(m), 1505(m), 1424(m), 1404(m), 1264(m), 1205(m), 1148(s), 1098(s), 1077(s), 1043(s), 1019(s), 949(m), 930(m), 870(s), 846(m), 823(m), 805(w), 558(s), 485(w), 467(m), 451(s). For compound **4**, tetrapropylammonium hydroxide was replaced with tetramethylammonium hydroxide (0.2 mmol, 0.260 mL), and the mixture was placed in a 15 mL Teflon-lined stainless steel vessel, heated to 200 °C in 2 h, kept there for 72 h, and then cooled to 25 °C at a rate of 5 °C/h. Yellow needlelike crystals were collected with some impurities as tablet crystals, which could be separated manually. Yield: 53% (based on uranium). IR (KBr, cm$^{-1}$): 3477 (b, s), 1637(m), 1516(m), 1487(m) 1421(w), 1400(w), 1261(m), 1201(w), 1140(s), 1109 (vs), 1090(vs), 1070(vs), 1032(vs), 1011(vs), 945(s), 908(s), 858(w), 806(m), 754(w), 694(w), 619(w), 545(m), 527(w), 478(w).

**Crystallographic Studies.** Crystals of four compounds were mounted on Cryoloops with paratone and optically aligned on a Bruker D8-Venture single-crystal X-ray diffractometer equipped with a digital camera. The diffraction data were collected using a Turbo X-ray Source (Mo K$\alpha$ radiation, $\lambda$ = 0.710 73 Å) adopting the direct-drive rotating anode technique and a CMOS detector under 100 K. The structures were solved by the direct method and refined on $F^2$ by full-matrix least-squares methods using SHELXTL.[17] All the non-hydrogen atoms were refined anisotropically. All the hydrogen atoms except those attached to water molecules were put in calculated positions. The hydrogen atoms of water molecules were found from the Fourier maps.



DOI: 10.1021/acs.inorgchem.5b00024
*Inorg. Chem.* 2015, 54, 3864−3874

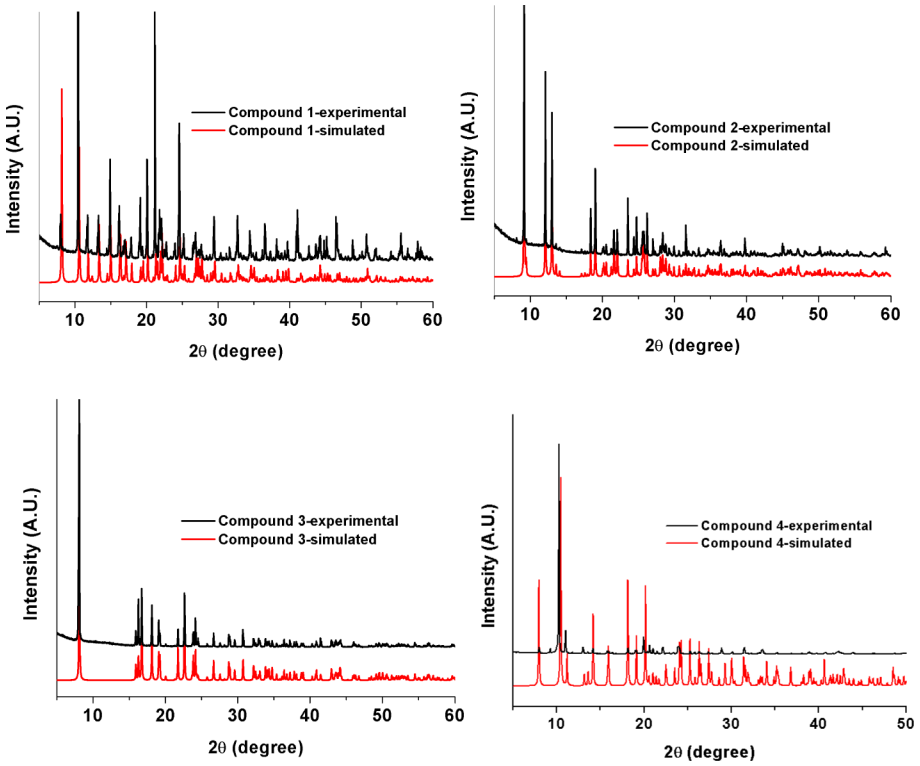


**Figure 1.** Simulated and experimental PXRD patterns of compounds **1**−**4** confirming their phase purities.

**Table 1. Crystal Data and Refinement Details for $[TPA][UO_2(pmbH_3)(pmbH_2)H_2O]\cdot 2H_2O$ (1), $[NH_4]_2[UO_2(pmb)]$ (2), $UO_2(pmbH_2)$ (3), and $[TMA]_2[(UO_2)_2(pmb)(HPO_3)]$ (4)**

| | 1 | 2 | 3 | 4 |
|---|---|---|---|---|
| formula | $C_{28}H_{55}NO_{17}P_4U$ | $C_8H_8N_2O_8P_2U$ | $C_8H_{10}O_8P_2U$ | $C_{16}H_8N_2O_{14}P_3U_2$ |
| M | 1039.67 | 560.13 | 534.13 | 1021.21 |
| crystal system | orthorhombic | triclinic | monoclinic | orthorhombic |
| Space group | $P2_12_12_1$ | $P\bar{1}$ | $P2_1/c$ | $Cmcm$ |
| $a$/Å | 14.224(1) | 7.983(1) | 10.947(1) | 7.042(1) |
| $b$/Å | 16.652(1) | 9.856(2) | 6.467(1) | 16.892(3) |
| $c$/Å | 16.678(1 | 10.039(2) | 9.275(1) | 22.154(4) |
| $\alpha$/deg | 90 | 88.592(5) | 90 | 90 |
| $\beta$/deg | 90 | 74.351(5) | 96.381(3) | 90 |
| $\gamma$/deg | 90 | 72.027(5) | 90 | 90 |
| $V$/Å$^3$ | 3950.4(5) | 722.0(2) | 652.6(1) | 2635.3(8) |
| $Z$ | 4 | 2 | 2 | 4 |
| $\rho_{calcd}$/g cm$^{-3}$ | 1.738 | 2.604 | 2.718 | 2.574 |
| $F(000)$ | 2048 | 520 | 552 | 1836 |
| $\mu$(Mo K$\alpha$)/mm$^{-1}$ | 4.34 | 11.508 | 12.712 | 12.524 |
| GOF on $F^2$ | 0.951 | 1.154 | 1.128 | 1.049 |
| $R_1$, $wR_2$ $[I > 2\sigma(I)]$ | 0.0435, 0.1123 | 0.0297, 0.0617 | 0.0223, 0.0669 | 0.0736, 0.1846 |
| $R_1$, $wR_2$ (all data)[a] | 0.0472, 0.1331 | 0.0419, 0.0786 | 0.0265, 0.0698 | 0.0746, 0.1851 |
| $(\Delta\rho)_{max}$, $(\Delta\rho)_{min}$/e Å$^{-3}$ | 1.721, −1.802 | 1.149, −1.400 | 0.855, −1.479 | 3.968, −7.206 |

[a] $R_1 = \sum||F_o| - |F_c||/\sum|F_o|$. $wR_2 = [\sum w(F_o^2 - F_c^2)^2/\sum w(F_o^2)^2]^{1/2}$

**Computational Details.** To elucidate the electronic structures of the crystals of compounds **1**−**3** and the binding modes of uranyl cation toward **pmb** ligands, theoretical studies were performed on these crystals using hybrid functional, B3LYP,[18] in Gaussian 09.[19] To simplify the computation, the molecular fragment was selected containing one uranyl cation and the surrounding ligands as a model. The two-component small-core quasi-relativistic effective core potentials (RECP), which replace 60 core electrons for uranium atom, were adopted here in combination with the corresponding basis set with a segmented contraction scheme.[20] Previous studies indicated that this level of theory could provide reliable results for uranium complexes.[21] Wiberg bond indices (WBIs) and electron density of the bond critical point were performed using Amsterdam density functional (ADF 2012) package.[22] B3LYP method and the Slater type orbital (STO) basis set with the quality of triple-$\zeta$ plus polarization (TZP)[23] basis set were used, without frozen core. The scalar relativistic (SR) effects were taken into account using the zero-order regular approximation (ZORA) approach.[24]

**Powder X-ray Diffraction.** Powder X-ray diffraction (PXRD) patterns were collected from 5° to 60°, with a step of 0.02°, and the data collection time was 0.5−1 s, using a Bruker D8 advance X-ray diffractometer with Cu K$\alpha$ radiation ($\lambda$ = 1.540 56 Å) equipped with a



DOI: 10.1021/acs.inorgchem.5b00024
*Inorg. Chem.* 2015, 54, 3864−3874

Lynxeye 1D detector. PXRD patterns of four compounds reveal that they are all single phases without any impurities.

**Thermal Stability.** Thermogravimetric analyses were performed on a NETZSCH STA 449F3 instrument in the range of 30−900 °C under a nitrogen flow at a heating rate of 10 °C/min for the first three compounds.

**UV−vis−near-IR, Fluorescence, and Raman Spectroscopy.** UV−vis−NIR (NIR = near-infrared) spectroscopy data were recorded from single crystals of four phases using a Craic Technologies microspectrophotometer. Fluorescence spectroscopy is collected with 365 nm wavelength excitation light. Crystals were placed on quartz slides, and the data were collected after optimization of microspectrophotometer. Raman spectra were collected with crystals placed on quartz slides without oil.

## RESULTS AND DISCUSSION

**Synthesis.** Compared to 1,4-phenylenebis(phosphonic acid), **pmbH$_4$** is more flexible as two methylene units are placed between the benzene ring and the two phosphonate groups, which is expected to lead to topologies of increased complexity. Using HF as a mineralizing agent, four compounds were obtained from the hydrothermal reactions of **pmbH$_4$** and $UO_2(NO_3)_2{\cdot}6H_2O$ with/without organic templates as pure phases proved by powder XRD results (Figure 1). Adjustment of the reaction conditions leads to diverse coordination modes of phosphonate ligand to the $UO_2^{2+}$ moiety.

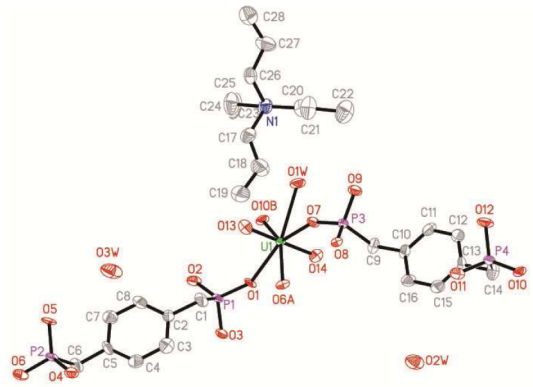


**Figure 2.** Asymmetric building unit of $[TPA][UO_2(pmbH_3)(pmbH_2)\text{-}H_2O]{\cdot}2H_2O$ (**1**) with atomic labeling scheme at 50% probability, and all hydrogen atoms are omitted for clarity.

**Table 2. Selected Bond Distances (Å) and Angles (deg) for $[TPA][UO_2(pmbH_3)(pmbH_2)H_2O]{\cdot}2H_2O$ (1)**

| | | | |
|---|---|---|---|
| U1≡O13 | 1.758(8) | P2−O6 | 1.487(9) |
| U1≡O14 | 1.781(9) | P2−O5 | 1.502(8) |
| U1−O1 | 2.339(7) | P2−O4 | 1.59(1) |
| U1−O7 | 2.347(9) | P3−O7 | 1.503(9) |
| U1−O6A | 2.357(9) | P3−O9 | 1.518(9) |
| U1−O10B | 2.382(8) | P3−O8 | 1.575(9) |
| U1−O1W | 2.542(9) | P4−O10 | 1.504(9) |
| P1−O1 | 1.503(8) | P4−O11 | 1.53(1) |
| P1−O2 | 1.528(9) | P4−O12 | 1.574(9) |
| P1−O3 | 1.546(8) | O13−U1−O10B | 90.2(4) |
| O13−U1−O14 | 178.9(4) | O14−U1−O10B | 88.8(4) |
| O13−U1−O1 | 90.0(4) | O1−U1−O10B | 74.8(3) |
| O14−U1−O1 | 90.1(4) | O7−U1−O10B | 134.4(3) |
| O13−U1−O7 | 91.3(4) | O6A−U1-O10B | 149.9(3) |
| O14−U1−O7 | 89.2(4) | O13−U1−O1W | 88.2(5) |
| O1−U1−O7 | 150.8(3) | O14−U1−O1W | 91.1(4) |
| O13−U1−O6A | 89.7(4) | O1−U1−O1W | 141.7(3) |
| O14−U1−O6A | 91.4(4) | O7−U1−O1W | 67.5(3) |
| O1−U1−O6A | 75.1(3) | O6A−U1−O1W | 143.1(3) |
| O7−U1−O6A | 75.7(3) | O10B−U1−O1W | 66.9(3) |

Symmetric codes for **1**: A: $x$ +1/2, $-y$ + 1/2, $-z$ + 2; B: $x$ − 1, $y$, $z$.

The temperature used for synthesizing **1** was different from that of other compounds. If the mixture was heated to 120 °C for 2 h and then cooled to 25 °C in 72 h, **1** could be collected as a pure phase. Increasing the temperature to 200 °C or extending the heating time to 120 h leads to the formation of **3**, even with tetrapropylammonium hydroxide. Therefore, it is reasonable to argue that **1** is a kinetic product, while **3** is thermodynamically more stable. In compound **4**, $pmbH_4$ ligands are partially decomposed to give phosphite unit, which cocoordinates to uranyl unit with $pmbH_4$ ligand, forming the first uranyl mixed phosphite/phosphonate compound.

**Structure Descriptions.** *Structure of $[TPA][UO_2(pmbH_3)\text{-}(pmbH_2)H_2O]{\cdot}2H_2O$ (**1**).* Compound **1** crystallizes in the chiral orthorhombic space group $P2_12_12_1$ (Table 1). The asymmetric unit contains one $UO_2^{2+}$ cation, two **pmb**, one $TPA^+$, one aqua ligand, and two lattice water molecules. As shown in Figure 2, the $UO_2^{2+}$ cation adopts a pentagonal bipyramid coordination geometry, forming a $UO_7$ unit. The U≡O and U−O bond lengths are in the range of 1.758(8)−1.781(9) Å and 2.339(7)−2.542(9) Å, respectively (Table 2). Five oxygen atoms located in the equatorial plane, O1, O7, O6A, O10B, and O1W, are from four **pmb** ligands and one aqua ligand, respectively. The U1−O1W bond distance is 2.542(9) Å. Therefore, **pmb** acts as a bridging ligand. There are two crystallographically independent **pmb** ligands: two phosphonate groups located at one side (type **I**) or each side (type **II**) of the benzene ring. Type **I** ligands string the $UO_7$ units to give chains, and type **II** ligands join two chains together with a zigzag style, forming a ribbon structure with negative charge (Figure 3). The overall structure was achieved by electrostatic attraction and van der Waals interaction, between negatively charged ribbons and $TPA^+$. The first $2_1$ screw axis runs along $a$ direction to give the ribbon structure; the other two $2_1$ screw axes are along the $b$ and $c$ directions, repeating the ribbon structure to yield the pseudo-3D structure.

The longest P−O bond distances in phosphonate group [P2−O4 is 1.59(1) Å, P3−O8 is 1.575(9) Å, and P4−O12 is 1.574(9) Å] are in agreement with P−O−H falling in the range of 1.56−1.63 Å, while P1−O3 is 1.546(8) Å, due to the delocalized proton (Table 2).[11a,13a,25] Interestingly, all coordinating oxygen atoms provided by the phosphonate group (O1, O6, O7, and O10) exhibit shortest distances [P1−O1 is 1.503(8) Å, P2−O6 is 1.487(9) Å, P3−O7 is 1.503(9) Å, and P4−O10 is 1.504(9) Å] with phosphor atoms in corresponding phosphonate groups, respectively, which means that all coordinating oxygen atoms are from P═O groups.[13a]

*Structure of $[NH_4]_2[UO_2(pmb)]$ (**2**).* Compound **2** crystallizes in the centrosymmetric triclinic space group $P\bar{1}$ (Table 1). The asymmetric unit contains one $UO_2^{2+}$ cation, two half **pmb** ligands, and two ammonium anions (Figure 4). Uranyl cation also adopts a pentagonal bipyramid coordination geometry, with five oxygen atoms located in the equatorial plane being O2, O3, O4, O6A, and O3B, from four **pmb** ligands, giving a $UO_7$ unit. The U≡O and U−O bond lengths are in the range of 1.778(5)−1.787(5) Å and 2.248(5)−2.560(5) Å, respectively (Table 3). There are two crystallographic different **pmb** ligands, acting as chelating and bridging ligands. Unlike compound **1**, there is only type **II** ligand. Dimers were


DOI: 10.1021/acs.inorgchem.5b00024
Inorg. Chem. 2015, 54, 3864−3874

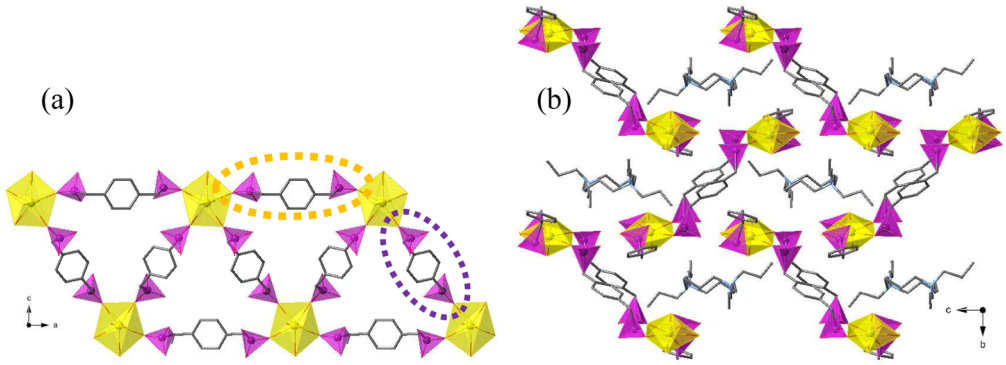


**Figure 3.** Ribbon structure (a) and 3D packing structure (b) of $[TPA][UO_2(pmbH_3)(pmbH_2)H_2O]\cdot 2H_2O$ (**1**) viewed along the *b* and *c* axes, respectively. $UO_7$ is represented by yellow pentagonal bipyramid, while $CPO_3$ is shown as purple tetrahedron. The **pmb** ligand in yellow elliptical ring is type **I**, and purple is type **II**.

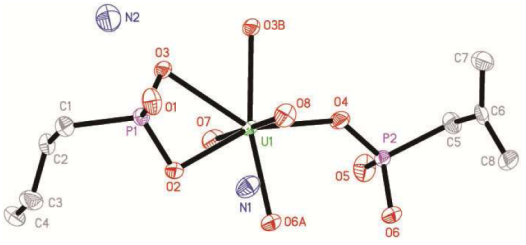


**Figure 4.** Asymmetric building unit of $[NH_4]_2[UO_2(pmb)]$ (**2**) with atomic labeling scheme at 50% probability, with all hydrogen atoms omitted for clarity.

**Table 3. Selected Bond Distances (Å) and Angles (deg) for $[NH_4]_2[UO_2(pmb)]$ (2)**

| | | | |
|---|---|---|---|
| U1≡O8 | 1.778(5) | P1−O1 | 1.502(5) |
| U1≡O7 | 1.787(5) | P1−O2 | 1.532(5) |
| U1−O6A | 2.248(5) | P1−O3 | 1.553(5) |
| U1−O4 | 2.307(5) | P2−O5 | 1.512(6) |
| U1−O3B | 2.378(5) | P2−O4 | 1.526(5) |
| U1−O2 | 2.428(5) | P2−O6 | 1.535(5) |
| U1−O3 | 2.560(5) | O8−U1−O2 | 84.4(2) |
| O8−U1−O7 | 179.1(2) | O7−U1−O2 | 95.0(2) |
| O8−U1−O6A | 94.3(2) | O6A−U1−O2 | 76.6(2) |
| O7−U1−O6A | 86.3(2) | O4−U1−O2 | 156.9(2) |
| O8−U1−O4 | 87.0(2) | O3B−U1−O2 | 121.3(2) |
| O7−U1−O4 | 93.7(2) | O8−U1−O3 | 89.1(2) |
| O6A−U1-O4 | 82.7(2) | O7−U1−O3 | 89.9(2) |
| O8−U1−O3B | 90.2(2) | O6A−U1-O3 | 133.7(2) |
| O7−U1−O3B | 89.5(2) | O4−U1−O3 | 143.7(2) |
| O6A−U1−O3B | 161.9(2) | O3B−U1−O3 | 63.8(2) |
| O4−U1−O3B | 80.1(2) | O2−U1−O3 | 57.7(2) |

Symmetric codes for **2**: A: $-x, -y + 2, -z + 2$; B: $-x, -y + 1, -z + 2$.

achieved by edge-sharing of two $UO_7$ units, with two $\mu_3$-O3 constituted the edge. The dimers were further connected to a chain via corner-sharing with phosphonate tetrahedrons. The **pmb** ligands are bridging between the chains of $UO_7$ and $CPO_3$ to construct the wavelike layers (Figure 5). The 3D structure was obtained by hydrogen bonds and van der Waals interactions between layers. The O1 and O5, which represent the shortest P−O distances in each phosphonate group [P1−O1 is 1.502(5) Å, and P2−O5 is 1.512(6) Å] do not belong to the P−O−U coordinated environment, so they were assigned to be from P═O bonds.

*Structure of $UO_2(pmbH_2)$ (**3**).* Compound **3** crystallizes in the centrosymmetric monoclinic space group $P2_1/c$ (Table 1).[26] The asymmetric unit contains a half $UO_2^{2+}$ cation and a half **pmb** ligand (Figure 6). Uranyl cation adopts a tetragonal bipyramid coordination geometry, with four oxygen atoms located in the equatorial plane (O1, O1A, O2B, and O2C), provided by four **pmb** ligands, forming a $UO_6$ unit. The U≡O bond length is 1.780(3), and the U−O bond lengths are 2.265(3) and 2.282(3) Å, respectively (Table 4). Like compound **2**, only type **II** ligand exists in compound **3**. The layer of $UO_6$ and $CPO_3$ was achieved by corner-sharing of tetragonal bipyramids and tetrahedrons (Figure 7). Then, they were linked by organic moiety of **pmb** ligands to give a 3D structure. The P1−O3 bond is protonated judging from its longest bond distance.

*Structure of $[TMA]_2[(UO_2)_2(pmb)(HPO_3)]$ (**4**).* Compound **4** crystallizes in the centrosymmetric orthorhombic space group *Cmcm* (Table 1). The asymmetric unit contains a half $UO_2^{2+}$ cation, a quarter **pmb** ligand, a quarter phosphite ligand, and a half tetramethylammonium cation (Figure 8). Uranyl cation adopts a tetragonal bipyramid coordination geometry similar to compound **3**, with four oxygen atoms located in the equatorial plane (O2, O3, O1A, and O1B), provided by three **pmb** ligands and one disordered phosphite ligand, forming a $UO_6$ unit. The U≡O bond length is in the range of 1.775(17)−1.776(18) Å, and the U−O bond length is in the range of 2.242(15)−2.275(14) Å, respectively (Table 5). Unlike other compounds, only type **I** ligands exist in compound **4**. The layer is built by corner-sharing of $UO_6$ tetragonal bipyramids and $CPO_3$ tetrahedra (Figure 9). Disordered tetramethylammonium cations are filled between layers to give a pseudo-3D structure.

**Summary of Bonding Modes.** The pH for compounds **1** and **3**, before and after hydrothermal reactions, changed subtly; mode **A** and **B** in Scheme 2 were found in compound **1** with P═O coordinating to uranium, while compound **2** changed dramatically, since the urea decomposed at high temperature to offer ammonia, resulting in all deprotonated P−O groups, where both mode **C** and **D** were displayed. In compound **3**, as the pH changed subtly and was kept acidic, one of P−O−H was deprotonated, showing bonding mode **E**; finally, in compound **4**, only mode **F** was found, where all phosphono oxygen atoms are bonded to uranium centers. A key message summarized here is that when $P-O^-$ bonds are protonated, P═O oxygen will mostly dominate the uranyl equatorial coordination (modes **A** and **B**), while P═O oxygen atoms lost their coordinating chance when $P-O^-$ is fully deprotonated


DOI: 10.1021/acs.inorgchem.5b00024
*Inorg. Chem.* 2015, 54, 3864−3874

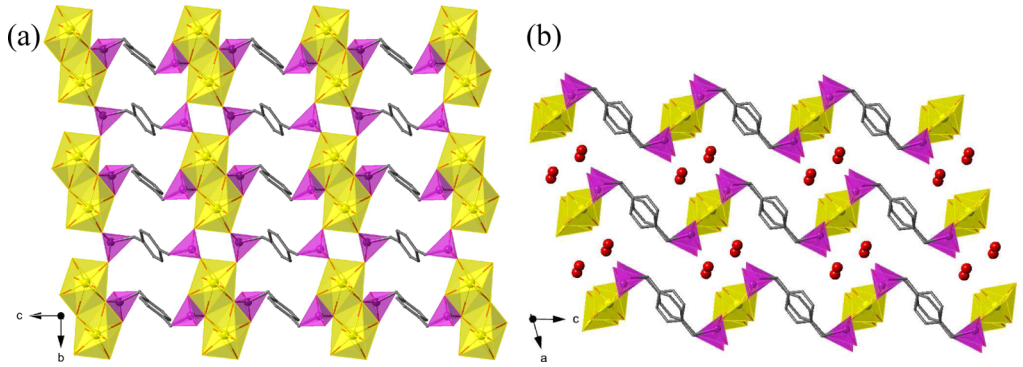


**Figure 5.** Layer structure (a) and 3D packing structure (b) of $[NH_4]_2[UO_2(pmb)]$ (**2**). $UO_7$ was represented by yellow pentagonal bipyramid, $CPO_3$ was purple tetrahedron, and ammonium anions (red ball) filled between layers were omitted.

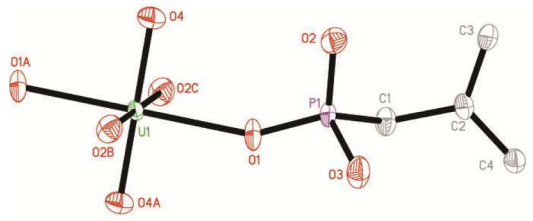


**Figure 6.** Asymmetric building unit of compound $UO_2(pmbH_2)$ (**3**) with atomic labeling scheme at 50% probability, and all hydrogen atoms are omitted for clarity.

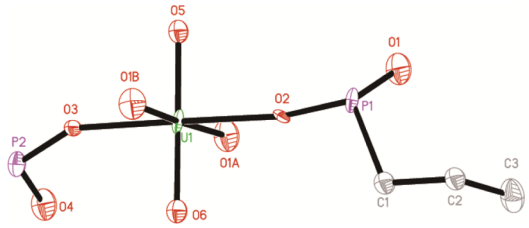


**Figure 8.** Asymmetric building unit of compound $[TMA]_2[(UO_2)_2(pmb)(HPO_3)]$(**4**) with atomic labeling scheme at 50% probability. All hydrogen atoms and TMA cation are omitted for clarity.

**Table 4. Selected Bond Distances (Å) and Angles (deg) for $UO_2(pmbH_2)$ (3)**

| | | | |
|---|---|---|---|
| U1≡O4 | 1.780(3) | P1−O1 | 1.505(3) |
| U1−O1 | 2.265(3) | P1−O2 | 1.507(3) |
| U1−O2B | 2.282(3) | P1−O3 | 1.569(4) |
| O4A−U1−O4 | 180 | O1A−U1−O2B | 89.1(1) |
| O4A−U1−O1 | 90.0(1) | O2B−U1−O2C | 180.0(1) |
| O1−U1−O1A | 180 | O1−P1−O2 | 113.7(2) |
| O4A−U1−O2B | 90.0(1) | O1−P1−O3 | 109.9(2) |
| O1−U1−O2B | 90.9(1) | O2−P1−O3 | 110.0(2) |

Symmetric codes for **3**: A: $-x + 1, -y, -z$; B: $-x + 1, y - 1/2, -z + 1/2$; C: $x, -y + 1/2, z - 1/2$.

**Table 5. Selected Bond Distances (Å) and Angles (deg) for $[TMA]_2[(UO_2)_2(pmb)(HPO_3)]$ (4)**

| | | | |
|---|---|---|---|
| U1≡O5 | 1.775(17) | U1−O1A | 2.275(14) |
| U1≡O6 | 1.776(18) | P1−O1 | 1.530(14) |
| U1−O2 | 2.242(15) | P1−O2 | 1.539(16) |
| U1−O3 | 2.270(16) | O2−U1−O3 | 179.2(6) |
| O5−U1−O6 | 179.6(8) | O5−U1−O1A | 89.3(4) |
| O5−U1−O2 | 90.6(7) | O6−U1−O1A | 90.7(4) |
| O6−U1−O2 | 89.8(7) | O2−U1−O1A | 89.2(3) |
| O5−U1−O3 | 90.2(7) | O3−U1−O1A | 90.9(3) |
| O6−U1−O3 | 89.5(7) | O1A−U1−O1B | 177.8(7) |

(modes **C** and **D**). Therefore, the coordinating abilities of phosphonate ligands are provided mostly by P═O at low pH and P−O at high pH.

**Theoretical Calculation Results.** To understand the bonding nature between uranyl cation and **pmb** ligands, Wiberg bond indices (WBIs) and the electron density at

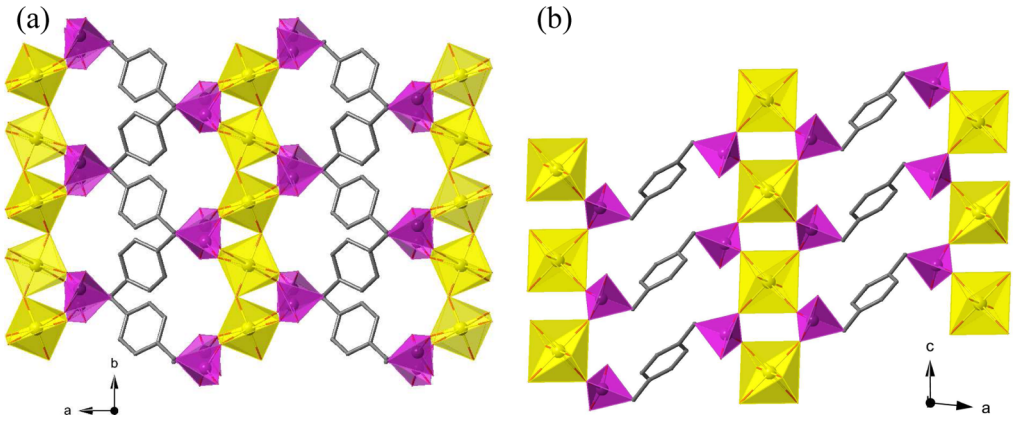


**Figure 7.** 3D structure of $UO_2(pmbH_2)$ (**3**) viewed along *c* (a) and *b* (b) axes. $UO_6$ was represented by yellow tetragonal bipyramid, while $CPO_3$ was purple tetrahedron.



DOI: 10.1021/acs.inorgchem.5b00024
*Inorg. Chem.* 2015, 54, 3864−3874

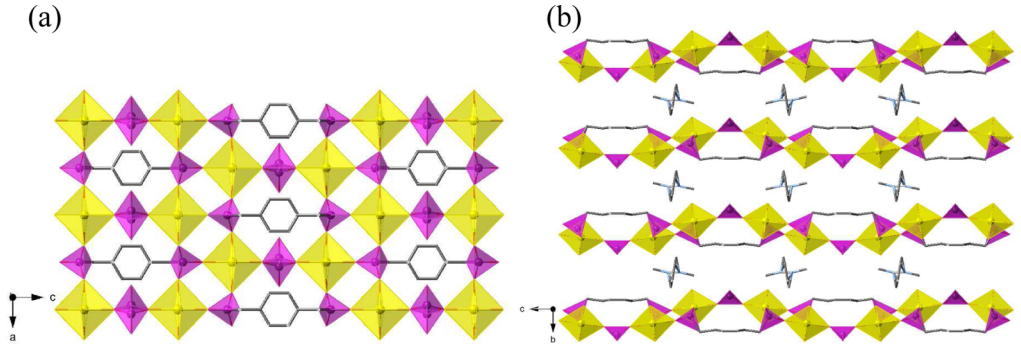


**Figure 9.** Layer and pseudo-3D structure of $[TMA]_2[(UO_2)_2(pmb)(HPO_3)]$(**4**) viewed along *b* (a) and *a* (b) axes, respectively. $UO_6$ was represented by yellow tetragonal bipyramid, whereas $CPO_3$ and $HPO_3$ were shown as purple tetrahedra. The disorder of $HPO_3^{2-}$ and $TMA^+$ is included in the figures.

**Scheme 2. Coordination Modes of Phosphonate Groups**[a]

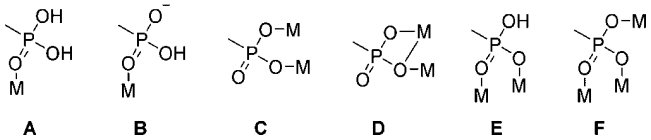


[a]Double bond of P═O was identified by bond distances.

**Table 6. Wiberg Bond Indices (WBIs) and the Electron Density [$\rho(r)$, a.u.] at Bond Critical Point for Compounds 1−3**

| compound **1** | WBIs | $\rho(r)$ | | WBIs | $\rho(r)$ |
|---|---|---|---|---|---|
| U1≡O13 | 2.196 | 0.305 | P2═O6 | 0.896 | 0.228 |
| U1≡O14 | 2.176 | 0.291 | P2−O5 | 1.212 | 0.230 |
| U1−O1 | 0.566 | 0.071 | P2−O4[a] | 0.640 | 0.184 |
| U1−O7 | 0.516 | 0.068 | P3═O7 | 0.875 | 0.221 |
| U1−O6A | 0.616 | 0.067 | P3−O9 | 0.792 | 0.216 |
| U1−O10B | 0.615 | 0.066 | P3−O8[a] | 0.777 | 0.196 |
| U1−O1W | 0.350 | 0.045 | P4═O10 | 1.017 | 0.225 |
| P1═O1 | 0.998 | 0.226 | P4−O11 | 1.185 | 0.219 |
| P1−O2[a] | 0.830 | 0.214 | P4−O12[a] | 0.777 | 0.196 |
| P1−O3[a] | 0.762 | 0.205 | | | |
| compound **2** | | | | | |
| U1≡O8 | 2.286 | 0.295 | P1═O1 | 1.268 | 0.231 |
| U1≡O7 | 2.275 | 0.290 | P1−O2 | 0.805 | 0.211 |
| U1−O6A | 0.708 | 0.068 | P1−O3 | 0.577 | 0.184 |
| U1−O4 | 0.842 | 0.081 | P2═O5 | 1.280 | 0.228 |
| U1−O3B | 0.339 | 0.140 | P2−O4 | 0.776 | 0.209 |
| U1−O2 | 0.708 | 0.068 | P2−O6 | 0.609 | 0.201 |
| U1−O3 | 0.335 | 0.047 | | | |
| compound **3** | | | | | |
| U1≡O4 | 2.182 | 0.290 | P1−O1 | 0.819 | 0.218 |
| U1−O1 | 0.724 | 0.085 | P1−O2 | 0.908 | 0.224 |
| U1−O2B | 0.561 | 0.080 | P1−O3[a] | 0.707 | 0.193 |

[a]the O atoms are protonated.

bond critical point were investigated (Table 6) for the first three compounds.

In compound **1**, it is interesting to note that for oxygen atoms that are involved in U−O bonding, the WBIs values of the corresponding P−O bonds (P1═O1, P2═O6, P3═O7, and P4═O10) are in the range of 0.875−1.017 Å, relatively large among all P−O bonds that are in the range of 0.640−0.792 Å (except P2−O5 and P4−O11 bonds), which confirms that all oxygen atoms coordinating to U1 are from P═O groups. O5, O9, and O11 are deprotonated oxygen atoms, for the fact that the value of $\rho(r)$ (P2−O5, 0.230; P3−O9, 0.216; P4−O11, 0.219) is larger than that of other P−O single bonds. The WBIs value of U1−O1W is 0.350, indicating that weak

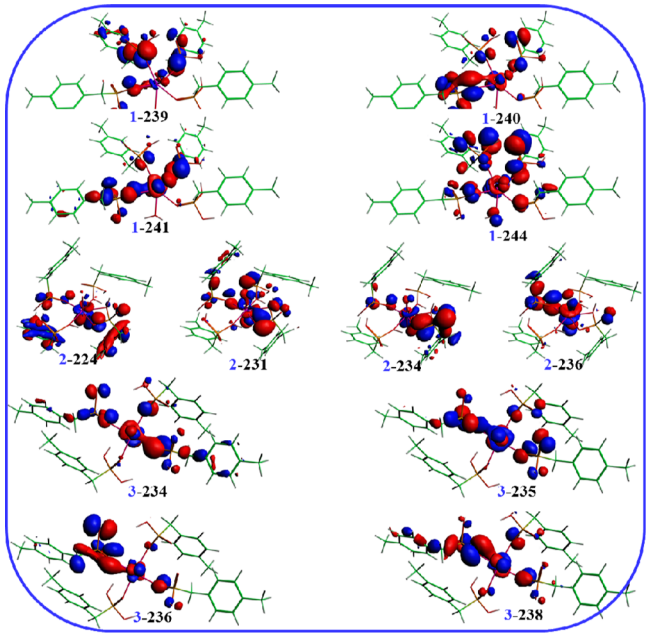


**Figure 10.** Selected molecular orbitals between the uranium atom and the **pmb** ligands for the compounds **1**−**3**.

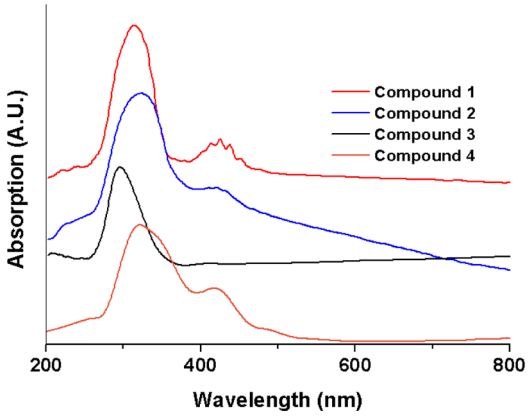


**Figure 11.** Absorption spectra of compound **1** (red), **2** (blue), **3** (black), and **4** (yellow).



DOI: 10.1021/acs.inorgchem.5b00024
*Inorg. Chem.* 2015, 54, 3864−3874

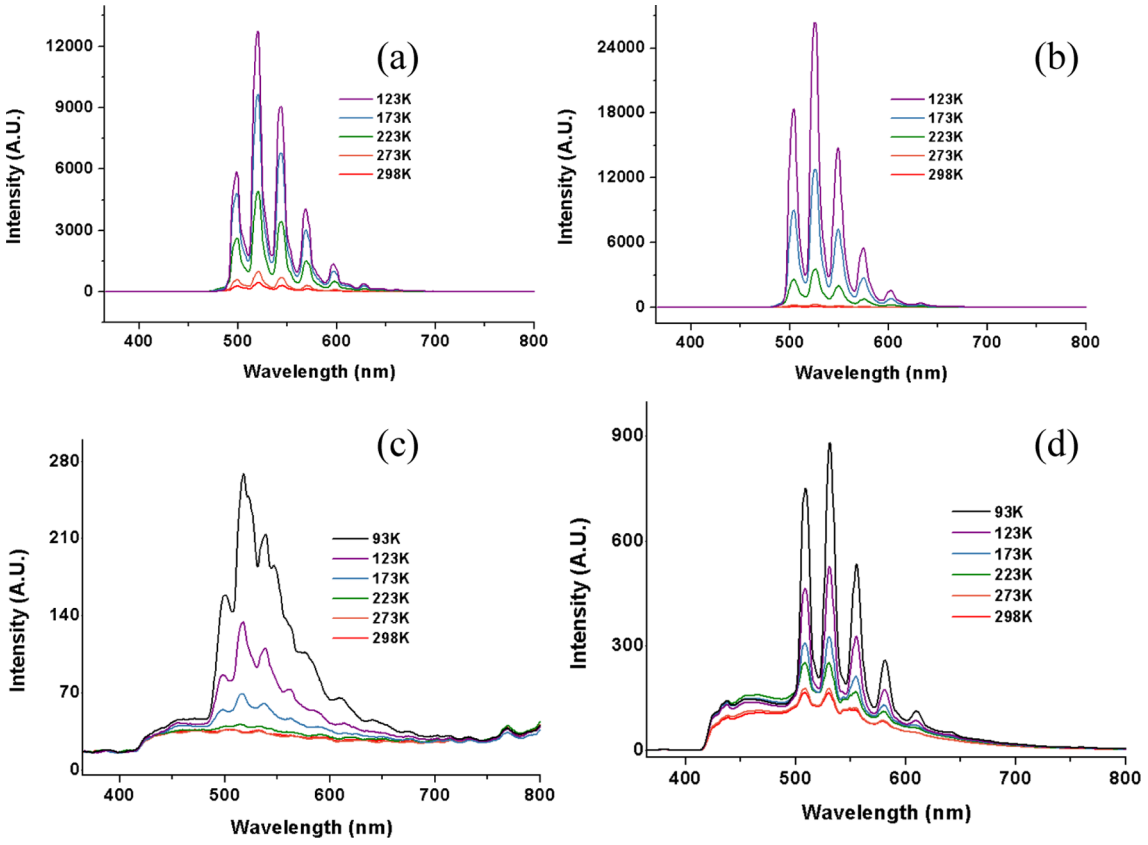


**Figure 12.** Viable temperature fluorescence spectra of compound **1** (a), **2** (b), **3** (c), and **4** (d).

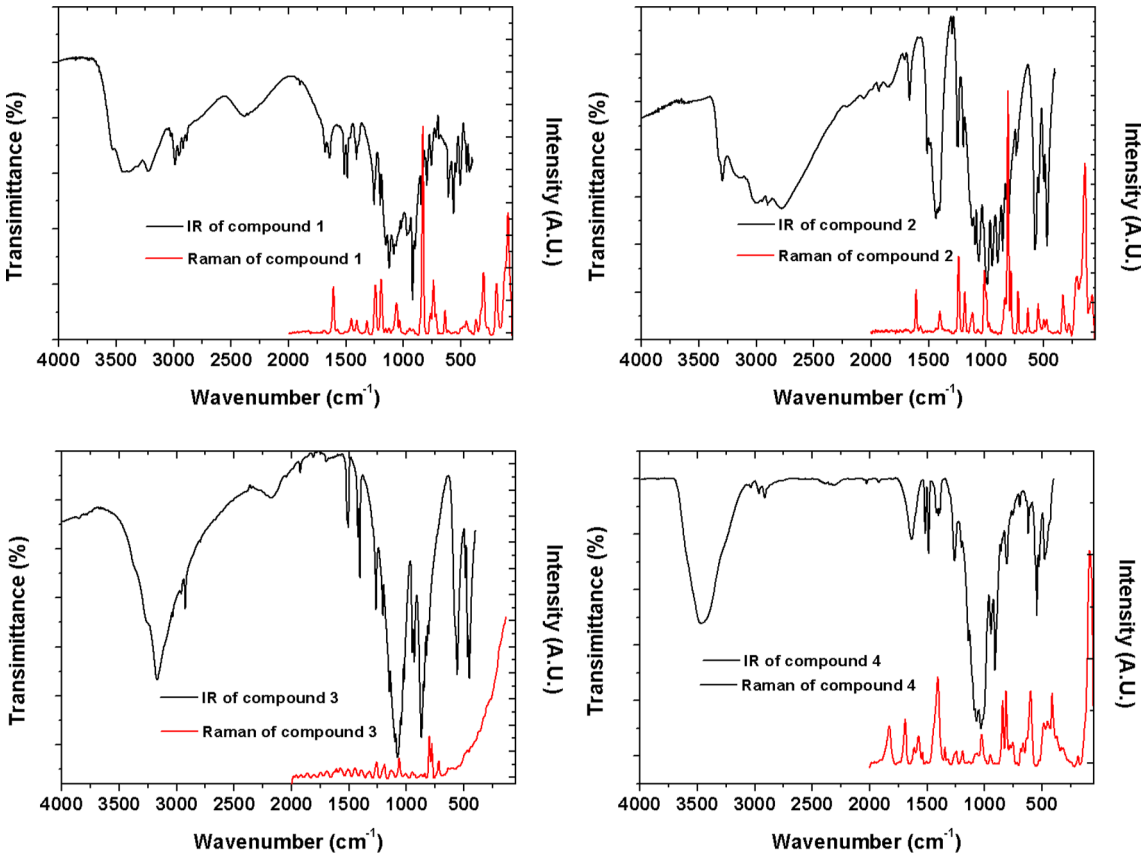


**Figure 13.** IR and Raman spectra of compounds **1**, **2**, **3**, and **4**.



DOI: 10.1021/acs.inorgchem.5b00024
*Inorg. Chem.* 2015, 54, 3864−3874

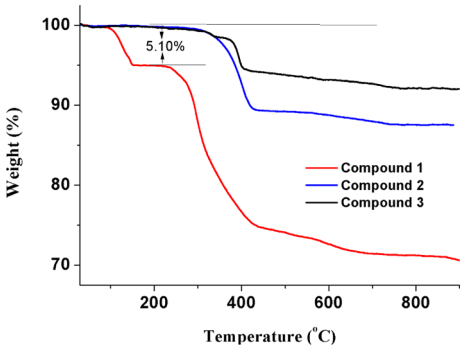


**Figure 14.** Thermogravimetric curves of compounds **1**, **2**, and **3**.

covalence is included, while other U−O bonds are in the range of 0.516−0.616 Å, suggesting that the interactions between P═O oxygen atoms and uranium centers are stronger compared to that of U1−O1W bond. This result is very consistent with the trend of the U−O bond from crystal structure data, where the U1−O1W bond distance is the longest among all U−O bonds in the equatorial plane.

For compound **2**, compared to all P−O bonds, the P1−O1 and P2−O5 bonds possess the largest WBIs values (1.268, 1.280), in accordance with the fact that the P1−O1 and P2−O5 bonds are the shortest distances in each phosphonate group and are assigned to double bonds. This is well-agreed with the crystal structure data.

As for compound **3**, the WBIs value of P1−O3 is the smallest among the three P1−O bonds, which reveals that the P1−O3 bond is the longest and that O3 is protonated. The WBIs values for P1−O1 and P1−O2 bonds are similar, deducing that O1−P−O2 plane is conjugated. The WBIs value for U1−O1 is larger than U1−O2, indicating that the strength of the U−O1 is higher than that of U−O2.

In addition, the electron density at bond critical point can also embody the interaction and bonding nature between two bonding atoms. On the basis of the electron density analysis, the trends of the U−O and P−O bonds are consistent with the results of the WBIs, respectively. The canonical valence molecular orbitals (MOs) relevant to the uranyl cation and ligands are provided in Figure 10. It should be pointed out that the MOs have $\sigma$ characters and are mainly contributed by the oxygen atom p orbital of the phosphonate group and the f and d orbitals of the uranium atoms.

**Spectroscopic Properties.** The UV−vis−NIR spectra of four compounds are shown in Figure 11. The peaks near 310 nm (314 for compound **1**, 324 for **2**, 294 for **3**, and 319 for **4**) and 420 nm are assigned to the equatorial U−O and the axial U≡O charge transfer, respectively, with vibration coupling.[10a] The peaks around 420 nm for compound **1** split into the peaks positioned at 390, 401, 413, 425, 437, and 450 nm, while for compound **2** splitting is not clear; splitting is not observed for compounds **3** or **4**. The baseline of compounds **1**, **3**, and **4** beyond 500 nm is virtually flat, while compound **2** shows a sloping shoulder, due to the light scattering of a particular chromophore.[25]

The charge-transfer based emission of yellow-green light around 525 nm is mainly due to lowest unoccupied molecular orbital−highest occupied molecular orbital electronic transitions coupled with symmetric and antisymmetric stretch vibrations of the nearly linear O≡U≡O unit.[10a,13c,d,27] As shown in Figure 12, Compound **1** show several peaks at 499(m), 521(s), 545(s), 570(w), and 598(vw) nm, while peaks for compound **2** are at 505(s), 526(s), 550(m), 575(w) and 604(vw) nm, typically observed in uranyl compounds.[13a,28] Compound **3** possesses much weaker luminescence signals at room temperature, likely attributed to the strict central symmetry of the uranyl site, resulting in that the excitation of lower state electron of uranium is Laporte-forbidden. This is also clearly shown in its absorption spectrum (Figure 11). Notably, the intensities of fluorescence spectra of all compounds increase with the decrease of temperature. Several peaks [500(s), 518(vs), 539(s), 547(m), 562(m), 578(w), and 610(w) nm] of compound **3** were observed at 93 K clearly. This is likely due to the inhibition of nonradiative emission quenching at low temperature. Compound **4** also shows five peaks located at 508(s), 531(vs), 555(m), 581(w), and 610(vw), but there is a broad feature present between 400 and 500 nm, likely due to the disordering shown in the structure.

Infrared (IR) and Raman spectra were also recorded for four compounds (Figure 13). Within IR spectra, the peaks between 3600 and 2600 $cm^{-1}$ are mainly assigned to the stretch of O−H from phosphonates and water molecules. The peaks appearing in the range of 1620−1400 $cm^{-1}$ are assigned to the stretch of benzene ring. The typical antisymmetric and symmetric stretch peaks of P═O and P−O in the range of 1210−990 $cm^{-1}$ are observed in these compounds.[25] The antisymmetric and symmetric stretch peaks of O≡U≡O are active in IR and Raman, respectively, and therefore are assigned (920 and 831 $cm^{-1}$ for **1**; 945 and 810 $cm^{-1}$ for **2**, 932 and 802 $cm^{-1}$ for **3**; 945 and 812 $cm^{-1}$ for **4**).

**Thermal Stability Measurement.** Thermal analysis shows that compound **1** begins to lose weight in the range of 90−150 °C and is stable between 150 and 240 °C, with 5.10% weight loss, corresponding to the loss of one coordination water and two lattice water (calcd 5.19%). When the temperature is beyond 240 °C, the structure of **1** collapsed. As compounds **2** and **3** have no water molecules in the structure, both are thermally stable up to 300 °C and then decompose with the collapse of the structure (Figure 14).

## CONCLUSIONS

The foregoing results demonstrate a trend of the coordinating competition between P═O and P−O$^-$ toward hexavalent uranyl units. Specifically, when phosphonic groups in pmb ligand are fully or partially protonated, the equatorial planes of uranyl units are mostly coordinated with P═O groups, while only P−O$^-$ binds to uranyl when phosphonic groups are fully deprotonated. These observations suggest that P═O groups would substantially outcompete with P−O groups to coordinate with uranyl ions at low pH, while the situation is reversed at high pH. Moreover, this bonding trend results in all structural dimensions including 1D chain, 2D layer, and 3D framework using the same ligand, which is uncommon in the uranyl phosphonate system. The DFT electronic structure calculation confirms the P−O−U and P═O−U bonding modes and provides some insights into their bonding nature. In addition, the fact that the chain compound **1** could convert to compound **3** with higher symmetry upon longer heating or higher reaction temperature implies that the **3** is thermally more stable, which is indicated by thermogravimetric results as well. Finally, the intensity change of absorption and fluorescence spectra from compounds **1** to **4** is consistent with their structural features. This result could shed light on the


DOI: 10.1021/acs.inorgchem.5b00024
*Inorg. Chem.* 2015, 54, 3864−3874

design of new phosphor based ligands for multiple nuclear industrial purposes.

## ■ ASSOCIATED CONTENT

### Supporting Information

X-ray crystallographic files, in cif format, for compounds **1**, **2**, **3**, and **4**. This material is available free of charge via the Internet at http://pubs.acs.org.

## ■ AUTHOR INFORMATION


### Corresponding Authors

*E-mail: shuaowang@suda.edu.cn. (S.W.)
*E-mail: diwujuan@suda.edu.cn. (J.D.)
*E-mail: shiwq@ihep.ac.cn. (W.-Q.S.)

### Author Contributions

[Δ]These authors contributed equally.


### Notes

The authors declare no competing financial interest.

## ■ ACKNOWLEDGMENTS

We are grateful for funding supported by National Science Foundation of China (91326112, 21422704, 21471107, 81402628), the Science Foundation of Jiangsu Province (BK20140007, BK20140303), a Project Funded by the Priority Academic Program Development of Jiangsu Higher Education Institutions (PAPD), and "Young Thousand Talented Program" in China. Support for T.E.A.-S. was provided by the Chemical Sciences, Geosciences, and Biosciences Division, Office of Basic Energy Sciences, Office of Science, Heavy Elements Chemistry Program, U.S. Department of Energy, under Grant No. DE-FG02-13ER16414.

## ■ REFERENCES


(1) (a) Mehta, V. S.; Maillot, F.; Wang, Z.; Catalano, J. G.; Giammar, D. E. *Chem. Geol.* **2014**, *36* (4), 66. (b) Cheng, T.; Barnett, M. O.; Roden, E. E.; Zhuang, J. L. *Environ. Sci. Technol.* **2004**, *38* (22), 6059. (c) Wu, S.; Chen, F.; Simonetti, A.; Albrecht-Schmitt, T. E. *Environ. Sci. Technol.* **2010**, *44* (8), 3192. (d) Alessi, D. S.; Lezama-Pacheco, J. S.; Stubbs, J. E.; Janousch, M.; Bargar, J. R.; Persson, P.; Bernier-Latmani, R. *Geochim. Cosmochim. Acta* **2014**, *131*, 115.

(2) (a) Jerden, J. L.; Sinha, A. K.; Zelazny, L. *Chem. Geol.* **2003**, *199* (1−2), 129. (b) Belova, L. N.; Gorshkov, A. I.; Doinikova, O. A.; Sivtsov, A. V. *Dokl. Akad. Nauk* **1998**, *358* (2), 215. (c) Singh, A.; Ulrich, K.-U.; Giammar, D. E. *Geochim. Cosmochim. Acta* **2010**, *74* (22), 6324. (d) Sowder, A. G.; Clark, S. B.; Fjeld, R. A. *J. Radioanal. Nucl. Chem.* **2001**, *248* (3), 517.

(3) (a) Mincher, B. J.; Modolo, G.; Mezyk, S. P. *Solvent Extr. Ion Exch.* **2009**, *27* (1), 1. (b) Rao, P. R. V.; Kolarik, Z. *Solvent. Extr. Ion. Exc* **1996**, *14* (6), 955. (c) Nakashima, K.; Kubota, F.; Maruyama, T.; Goto, M. *Ind. Eng. Chem. Res.* **2005**, *44* (12), 4368. (d) ArnaudNeu, F.; Bohmer, V.; Dozol, J. F.; Gruttner, C.; Jakobi, R. A.; Kraft, D.; Mauprivez, O.; Rouquette, H.; SchwingWeill, M. J.; Simon, N.; Vogt, W. *J. Chem. Soc., Perkin Trans. 2* **1996**, No. 6, 1175. (e) Ansari, S. A.; Pathak, P. N.; Manchanda, V. K.; Husain, M.; Prasad, A. K.; Parmar, V. S. *Solvent Extr. Ion Exch.* **2005**, *23* (4), 463. (f) Romanovskiy, V. N.; Smirnov, I. V.; Babain, V. A.; Todd, T. A.; Herbst, R. S.; Law, J. D.; Brewer, K. N. *Solvent Extr. Ion Exch.* **2001**, *19* (1), 1.

(4) (a) Alsobrook, A. N.; Hauser, B. G.; Hupp, J. T.; Alekseev, E. V.; Depmeier, W.; Albrecht-Schmitt, T. E. *Chem. Commun.* **2010**, *46* (48), 9167. (b) Liao, Z.-L.; Li, G.-D.; Bi, M.-H.; Chen, J.-S. *Inorg. Chem.* **2008**, *47* (11), 4844. (c) Bao, S.-S.; Liao, Y.; Su, Y.-H.; Liang, X.; Hu, F.-C.; Sun, Z.; Zheng, L.-M.; Wei, S.; Alberto, R.; Li, Y.-Z.; Ma, J. *Angew. Chem.* **2011**, *123* (24), 5618. (d) Bao, S.-S.; Otsubo, K.; Taylor, J. M.; Jiang, Z.; Zheng, L.-M.; Kitagawa, H. *J. Am. Chem. Soc.* **2014**, *136* (26), 9292. (e) Adelani, P. O.; Albrecht-Schmitt, T. E. *Angew. Chem., Int. Ed.* **2010**, *49* (47), 8909.

(5) Bao, S.-S.; Chen, G.-S.; Wang, Y.; Li, Y.-Z.; Zheng, L.-M.; Luo, Q.-H. *Inorg. Chem.* **2006**, *45* (3), 1124.

(6) (a) Laintz, K. E.; Tachikawa, E. *Anal. Chem.* **1994**, *66* (13), 2190. (b) Lin, Y. H.; Wai, C. M. *Anal. Chem.* **1994**, *66* (13), 1971.

(7) Nakashima, K.; Kubota, F.; Maruyama, T.; Goto, M. *Anal. Sci.* **2003**, *19* (8), 1097.

(8) Powell, B. A.; Navratil, J. D.; Thompson, M. C. *Solvent Extr. Ion Exch.* **2003**, *21* (3), 347.

(9) (a) Chiarizia, R.; Horwitz, E. P.; Alexandratos, S. D.; Gula, M. J. *Sep. Sci. Technol.* **1997**, *32* (1−4), 1. (b) Chiarizia, R.; Horwitz, E. P.; Alexandratos, S. D. *Solvent Extr. Ion Exch.* **1994**, *12* (1), 211. (c) Horwitz, E. P.; Chiarizia, R.; Diamond, H.; Gatrone, R. C.; Alexandratos, S. D.; Trochimczuk, A. Q.; Crick, D. W. *Solvent Extr. Ion Exch.* **1993**, *11* (5), 943.

(10) (a) Adelani, P. O.; Albrecht-Schmitt, T. E. *J. Solid State Chem.* **2012**, *192* (0), 377. (b) Ramaswamy, P.; Prabhu, R.; Natarajan, S. *Inorg. Chem.* **2010**, *49* (17), 7927. (c) Nelson, A.-G. D.; Bray, T. H.; Stanley, F. A.; Albrecht-Schmitt, T. E. *Inorg. Chem.* **2009**, *48* (10), 4530. (d) Diwu, J.; Wang, S.; Liao, Z.; Burns, P. C.; Albrecht-Schmitt, T. E. *Inorg. Chem.* **2010**, *49* (21), 10074. (e) Bray, T. H.; Nelson, A.-G. D.; Jin, G. B.; Haire, R. G.; Albrecht-Schmitt, T. E. *Inorg. Chem.* **2007**, *46* (26), 10959. (f) Lin, J.; Cross, J. N.; Diwu, J.; Polinski, M. J.; Villa, E. M.; Albrecht-Schmitt, T. E. *Inorg. Chem.* **2012**, *51* (21), 11949. (g) Diwu, J.; Wang, S.; Good, J. J.; DiStefano, V. H.; Albrecht-Schmitt, T. E. *Inorg. Chem.* **2011**, *50* (11), 4842. (h) Diwu, J.; Nelson, A.-G. D.; Wang, S.; Campana, C. F.; Albrecht-Schmitt, T. E. *Inorg. Chem.* **2010**, *49* (7), 3337. (i) Diwu, J.; Grant, D. J.; Wang, S.; Gagliardi, L.; Albrecht-Schmitt, T. E. *Inorg. Chem.* **2012**, *51* (12), 6906.

(11) (a) Doran, M. B.; Norquist, A. J.; O'Hare, D. *Chem. Mater.* **2003**, *15* (7), 1449. (b) Poojary, D. M.; Grohol, D.; Clearfield, A. *J. Phys. Chem. Solids* **1995**, *56* (10), 1383. (c) Wu, H.-Y.; Ma, Y.-Q.; Zhang, X.; Zhang, H.; Yang, X.-Y.; Li, Y.-H.; Wang, H.; Yao, S.; Yang, W. *Inorg. Chem. Commun.* **2013**, *34* (0), 55. (d) Knope, K. E.; Cahill, C. L. *Inorg. Chem.* **2008**, *47* (17), 7660. (e) Knope, K. E.; Cahill, C. L. *Inorg. Chem.* **2009**, *48* (14), 6845. (f) Alsobrook, A. N.; Albrecht-Schmitt, T. E. *Inorg. Chem.* **2009**, *48* (23), 11079.

(12) (a) Yang, W.; Wu, H.-Y.; Wang, R.-X.; Pan, Q.-J.; Sun, Z.-M.; Zhang, H. *Inorg. Chem.* **2012**, *51* (21), 11458. (b) Wu, H.-Y.; Yang, W.; Sun, Z.-M. *Cryst. Growth Des.* **2012**, *12* (9), 4669.

(13) (a) Adelani, P. O.; Oliver, A. G.; Albrecht-Schmitt, T. E. *Cryst. Growth Des.* **2011**, *11* (5), 1966. (b) Adelani, P. O.; Albrecht-Schmitt, T. E. *J. Solid State Chem.* **2011**, *184* (9), 2368. (c) Adelani, P. O.; Albrecht-Schmitt, T. E. *Cryst. Growth Des.* **2011**, *11* (9), 4227. (d) Adelani, P. O.; Albrecht-Schmitt, T. E. *Cryst. Growth Des.* **2012**, *12* (11), 5800. (e) Adelani, P. O.; Albrecht-Schmitt, T. E. *Inorg. Chem.* **2009**, *48* (7), 2732.

(14) Yang, Y.; Wang, S.; Polinski, M. J.; Liu, Y.; Barnett, M. O.; Albrecht-Schmitt, T. E. *Chem. Geol.* **2013**, *357*, 67.

(15) (a) Howe, A. T.; Shilton, M. G. *J. Solid State Chem.* **1979**, *28* (3), 345. (b) Howe, A. T.; Shilton, M. G. *J. Solid State Chem.* **1980**, *34* (2), 149.

(16) Pramanik, M.; Nandi, M.; Uyama, H.; Bhaumik, A. *Green Chem.* **2012**, *14* (8), 2273.

(17) Sheldrick, G. M. *SHELXTL;* Siemens Analytical X-ray Instruments, Inc: Madison, WI, 2001.

(18) Lee, C. T.; Yang, W. T.; Parr, R. G. *Phys. Rev. B* **1988**, *37* (2), 785.

(19) Frisch, M. J.; Trucks, G. W.; Schlegel, H. B.; Scuseria, G. E.; Robb, M. A.; Cheeseman, J. R.; Scalmani, G.; Barone, V.; Mennucci, B.; Petersson, G. A.; Nakatsuji, H.; Caricato, M.; Li, X.; Hratchian, H. P.; Izmaylov, A. F.; Bloino, J.; Zheng, G.; Sonnenberg, J. L.; Hada, M.; Ehara, M.; Toyota, K.; Fukuda, R.; Hasegawa, J.; Ishida, M.; Nakajima, T.; Honda, Y.; Kitao, O.; Nakai, H.; Vreven, T.; Montgomery Jr., J. A.; Peralta, J. E.; Ogliaro, F.; Bearpark, M. J.; Heyd, J.; Brothers, E. N.; Kudin, K. N.; Staroverov, V. N.; Kobayashi, R.; Normand, J.; Raghavachari, K.; Rendell, A. P.; Burant, J. C.; Iyengar, S. S.; Tomasi, J.; Cossi, M.; Rega, N.; Millam, N. J.; Klene, M.; Knox, J. E.;




DOI: 10.1021/acs.inorgchem.5b00024
*Inorg. Chem.* 2015, 54, 3864−3874

Cross, J. B.; Bakken, V.; Adamo, C.; Jaramillo, J.; Gomperts, R.; Stratmann, R. E.; Yazyev, O.; Austin, A. J.; Cammi, R.; Pomelli, C.; Ochterski, J. W.; Martin, R. L.; Morokuma, K.; Zakrzewski, V. G.; Voth, G. A.; Salvador, P.; Dannenberg, J. J.; Dapprich, S.; Daniels, A. D.; Farkas, Ö.; Foresman, J. B.; Ortiz, J. V.; Cioslowski, J.; Fox, D. J. *Gaussian 09;* Gaussian, Inc.: Wallingford, CT, 2009.

(20) (a) Küchle, W.; Dolg, M.; Stoll, H.; Preuss, H. *J. Chem. Phys.* **1994**, *100* (10), 7535. (b) Cao, X.; Dolg, M.; Stoll, H. *J. Chem. Phys.* **2003**, *118* (2), 487. (c) Cao, X.; Dolg, M. *J. Mol. Struct.: THEOCHEM* **2004**, *673* (1−3), 203. (d) Wu, Q.-Y.; Lan, J.-H.; Wang, C.-Z.; Xiao, C.-L.; Zhao, Y.-L.; Wei, Y.-Z.; Chai, Z.-F.; Shi, W.-Q. *J. Phys. Chem. A* **2014**, *118* (11), 2149.

(21) (a) Lan, J.-H.; Shi, W.-Q.; Yuan, L.-Y.; Zhao, Y.-L.; Li, J.; Chai, Z.-F. *Inorg. Chem.* **2011**, *50* (19), 9230. (b) Wang, C.-Z.; Shi, W.-Q.; Lan, J.-H.; Zhao, Y.-L.; Wei, Y.-Z.; Chai, Z.-F. *Inorg. Chem.* **2013**, *52* (19), 10904. (c) Wu, Q.-Y.; Wang, C.-Z.; Lan, J.-H.; Xiao, C.-L.; Wang, X.-K.; Zhao, Y.-L.; Chai, Z.-F.; Shi, W.-Q. *Inorg. Chem.* **2014**, *53* (18), 9607.

(22) (a) Fonseca Guerra, C.; Snijders, J. G.; te Velde, G.; Baerends, E. J. *Theor. Chem. Acc.* **1998**, *99* (6), 391. (b) te Velde, G.; Bickelhaupt, F. M.; Baerends, E. J.; Fonseca Guerra, C.; van Gisbergen, S. J. A.; Snijders, J. G.; Ziegler, T. *J. Comput. Chem.* **2001**, *22* (9), 931.

(23) Van Lenthe, E.; Baerends, E. J. *J. Comput. Chem.* **2003**, *24* (9), 1142.

(24) Lenthe, E. v.; Baerends, E. J.; Snijders, J. G. *J. Chem. Phys.* **1993**, *99* (6), 4597.

(25) Grohol, D.; Clearfield, A. *J. Am. Chem. Soc.* **1997**, *119* (20), 4662.

(26) Monteiro, B.; Fernandes, J. A.; Pereira, C. C.; Vilela, S. M.; Tome, J. P.; Marçalo, J.; Almeida Paz, F. A. *Acta Crystallogr., Sect. B* **2014**, *70* (1), 28.

(27) Su, J.; Zhang, K.; Schwarz, W. H. E.; Li, J. *Inorg. Chem.* **2011**, *50* (6), 2082.

(28) (a) Zhu, Q.; Shang, R.; Chen, S.; Liu, C.; Wang, Z.; Gao, S. *Inorg. Chem.* **2014**, *53* (16), 8708. (b) Adelani, P. O.; Oliver, A. G.; Albrecht-Schmitt, T. E. *Cryst. Growth Des.* **2011**, *11* (7), 3072.



DOI: 10.1021/acs.inorgchem.5b00024
*Inorg. Chem.* 2015, 54, 3864−3874